

Intrinsic Electron Mobility Limits in β -Ga₂O₃

Nan Ma,^{1, a)} Nicholas Tanen,¹ Amit Verma,¹ Zhi Guo,² Tengfei Luo,² Huili (Grace) Xing,^{1,3} and Debdeep Jena^{1,3, b)}

¹⁾School of Electrical and Computer Engineering, Cornell University, Ithaca, NY 14853, USA.

²⁾Department of Aerospace and Mechanical Engineering, University of Notre Dame, Notre Dame, IN 46556, USA.

³⁾Department of Materials Science and Engineering, Cornell University, Ithaca, NY 14853, USA.

(Dated: 17 February 2022)

By systematically comparing experimental and theoretical transport properties, we identify the polar optical phonon scattering as the dominant mechanism limiting electron mobility in β -Ga₂O₃ to <200 cm²/V·s at 300 K for donor doping densities lower than $\sim 10^{18}$ cm⁻³. In spite of similar electron effective mass of β -Ga₂O₃ to GaN, the electron mobility is $\sim 10\times$ lower because of a massive Fröhlich interaction, due to the low phonon energies stemming from the crystal structure and strong bond ionicity. Based on the theoretical and experimental analysis, we provide an empirical expression for electron mobility in β -Ga₂O₃ that should help calibrate its potential in high performance device design and applications.

β -Ga₂O₃ has recently emerged as an ultra wide-bandgap semiconductor $E_g = 4.6 - 4.9$ eV^{1,2} with 300 K electron mobility $\mu \sim 150$ cm²/V·s,³ attractive enough to potentially offer high-voltage electronic device performance⁴ that is beyond the reach of the currently successful GaN and SiC platforms. With the recent success in the synthesis of large-area bulk single crystal substrates and availability of nanomembranes,⁴⁻⁶ β -Ga₂O₃ becomes a transparent conductive oxide (TCO) with significant potential. It advances the field of oxide electronics from the traditional IGZO, perovskites (SrTiO₃, BaSnO₃, etc), and ZnO.⁷⁻⁹ In this work, we have explored the physics of the intrinsic electron mobility limits in this material system and obtained expressions that should prove useful in device design.

Since the Drude electron mobility $\mu = e\tau/m_c^*$ is determined by the conduction band minimum (CBM) effective mass m_c^* , electron charge e , and the low-field scattering rate τ , we investigate m_c^* term first. From standard $\mathbf{k} \cdot \mathbf{p}$ theory, m_c^* of sp³-bonded direct gap semiconductors with the CBM at the Γ point is related to E_g by¹⁰ $m_c^*/m_0 \sim (1 + \frac{2p_0^2}{m_0 E_g})^{-1}$, where $p_0 \approx \hbar/a_0$ is the de-Broglie momentum of electrons at the Brillouin-zone edge $k = 2\pi/a_0$ with k the electron wavevector, a_0 the lattice constant, $\hbar = 2\pi\hbar$ the Planck's constant, and m_0 the free electron rest mass. Figure 1 (a) shows m_c^* for various compound semiconductors as a function of E_g .^{11,12} The solid blue line shows the $\mathbf{k} \cdot \mathbf{p}$ prediction with $2p_0^2/m_0 \sim 14$ eV. Variations in lattice constant, Landé g factor, slight indirectness of the bandgap, and the ionicity of the semiconductor can explain the slight deviations,¹⁰ but the overall fit and the trend it predicts overrides these details – with a large $E_g \sim 4.6 - 4.9$ eV,^{1,2} β -Ga₂O₃ boasts a relatively low $m_c^* \sim 0.23 - 0.28m_0$,^{2,13} as indicated in Fig. 1

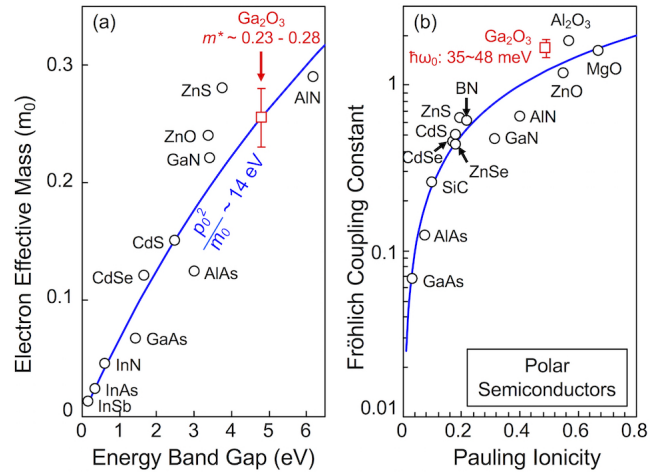


FIG. 1. (a) Electron effective mass versus energy band gap and (b) Fröhlich coupling constants versus Pauling ionicity for various compound semiconductors.

(a). Unlike several other complex oxides and perovskites, where $|d\rangle$ or $|p\rangle$ orbital conduction bands lead to heavy m_c^* , β -Ga₂O₃ has a small m_c^* because the CBM electron states derive from the hybridization of the Ga $|s\rangle$ orbitals. Now because m_c^* of β -Ga₂O₃ is similar to that of GaN, one may initially expect the 300 K Drude mobility to be similar to bulk GaN (~ 1500 cm²/V·s). However, the maximum experimentally measured 300 K electron mobility in bulk single-crystal β -Ga₂O₃ with little or no dislocations is $\sim 110-150$ cm²/V·s,^{3,6,14-16} nearly an order of magnitude lower than GaN. Potential electronic device applications of β -Ga₂O₃ beg the question whether the reported lower mobilities are intrinsic, or can be improved by eliminating extrinsic defects. Answering this question is the subject of this work.

We turn to the scattering rate to explain the difference in mobility between GaN and β -Ga₂O₃. Because the Ga-O bond is strongly ionic,¹⁷ one can expect po-

^{a)}Electronic mail: nanma@cornell.edu.

^{b)}Electronic mail: djena@cornell.edu.

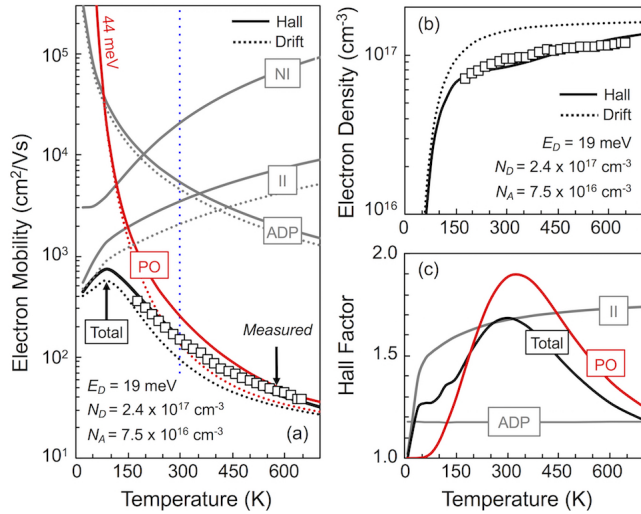


FIG. 2. Temperature-dependent (a) electron mobility, (b) electron density, and (c) Hall factors in β -Ga₂O₃. The solid and dashed lines in (a) and (b) indicate Hall and drift electron mobilities (densities), respectively. The open squares indicate experimental results obtained using Hall-effect measurements.

lar optical (PO) phonons to play an important role in limiting the room-temperature electron mobility, similar to GaN and GaAs.^{18,19} The PO phonon energy $\hbar\omega_0$ intersects the electron bandstructure at the characteristic wavevector $k_0 = \sqrt{2m_c^* \omega_0 / \hbar}$, which defines a characteristic Born-effective field²⁰ $E_0 = \frac{e^2}{4\pi\epsilon_0} \frac{k_0^2}{2} \left(\frac{1}{\epsilon_\infty} - \frac{1}{\epsilon_s} \right)$, where ϵ_0 is the vacuum permittivity, and ϵ_s and ϵ_∞ are the low- and high-frequency relative dielectric constant of the semiconductor. For polar semiconductors, the strength of electron-PO phonon (e-PO) interaction is dictated by the dimensionless Fröhlich coupling constant:²¹

$$\alpha_F = \frac{eE_0/k_0}{\hbar\omega_0} = \frac{e^2}{8\pi\epsilon_0\hbar} \sqrt{\frac{2m_c^*}{\hbar\omega_0}} \left(\frac{1}{\epsilon_\infty} - \frac{1}{\epsilon_s} \right) \quad (1)$$

Figure. 1 (b) shows α_F for several polar semiconductors plotted against their Pauling ionicity: $f_p = 1 - \exp[-(X_{AB})^2/4]$ ²², where X_{AB} is the difference of the electronegativity of the two elements in the bond. The blue solid trend line shows the empirical relation $\alpha_F \sim 2.5 \times f_p$, showing that α_F increases with f_p , i.e., strongly ionic bonds lead to stronger e-PO interaction. Recent polarized reflectance measurements performed by Onuma et al.²³ show that the lowest optical phonon modes $\hbar\omega_0$ in β -Ga₂O₃ are in the range of 35-48 meV, which leads to $\alpha_F \sim 1.68 \pm 0.21$, as shown by the red open square in Fig. 1 (b). This indicates a massive Fröhlich coupling, nearly $3\times$ stronger than GaN. Polaron effects, such as self-trapped holes due to their heavy band,²⁴ can be expected to be strong in β -Ga₂O₃, renormalizing the electron effective mass $m_p^*/m_c^* \sim (1 + \alpha_F/6)$,²⁰ which is used in the following transport properties study.

For non-degenerate dilute carrier densities at high temperatures (T) when $\hbar\omega_0/k_B T \ll 1$, where k_B is the Boltz-

mann constant, the PO phonon scattering limited electron mobility²⁵ $\mu_{PO} \propto [\exp(\hbar\omega_0/k_B T) - 1]/\omega_0 \alpha_F$. From the 300 K $\mu_{PO} \sim 1500$ cm²/V·s of bulk GaN, one can estimate μ_{PO} in β -Ga₂O₃ to be ~ 88 -141 cm²/V·s. This value agrees with the reported $\mu \sim 110$ -150 cm²/V·s in β -Ga₂O₃ at 300 K.^{3,6,14-16} This simple analysis indicates that PO phonon is likely the dominant room-temperature scattering mechanism in β -Ga₂O₃ and rules out other possibilities of intrinsic scattering mechanisms.

Hall-effect measurements were performed over a wide temperature range from 180 K to 650 K using a Lakeshore Hall system on unintentionally-doped Ga₂O₃ bulk substrates from Tamura Corporation. These substrates were diced into 5 mm \times 5 mm square pieces. Ti/Pt Ohmic contacts were deposited on the four corners of the sample in Van de Pauw geometry followed by rapid thermal annealing (2 min, 480 °C, Nitrogen atmosphere). Figure 2 (a) shows the measured temperature-dependent electron mobilities in β -Ga₂O₃, and Figure 2 (b) shows the measured electron density, both as open squares. The lines in Figure 2 (a) show the calculated mobility resolved into the individual scattering mechanisms by ADP (μ_{ADP}), ionized (μ_{II}) and neutral impurity (μ_{NI}) scattering, and the red line shows the polar-optical scattering limited mobility μ_{PO} . These calculations are described after a brief discussion. The solid line in Figure 2 (b) is the calculated Hall-effect carrier density n_H based on the Hall mobility μ_H and the dashed line is n , corresponding to the drift mobility μ_d .

Figure 2 (c) shows the calculated Hall-factor r_H due to each scattering mechanism and the net r_H with all scattering mechanisms considered, highlighting the difference between μ_H and μ_d . N_D , N_A , and the ionization energy E_D are from fitting of the temperature-dependent n using the neutrality condition: $n + N_A = N_D^+$. For the current sample, $N_D = 2.4 \times 10^{17}$ cm⁻³, $N_A = 7.5 \times 10^{16}$ cm⁻³, and $E_D = 19$ meV. Figure 2 (a) indicates that extrinsic scattering from ionized and neutral impurity dominate the electron mobility at low temperatures up to ~ 150 K. Among intrinsic scattering mechanisms, μ_{ADP} is higher than the measured mobility by more than one order of magnitude over the entire temperature range. Consequently the only mechanism that limits the electron mobility at high temperatures is PO phonon scattering. The optical phonon energy $\hbar\omega_0$ that explains the measured temperature-dependent μ_H is ~ 44 meV, which is very close to the lowest phonon energies from optical spectroscopy measurements reported by Onuma et al.²³ It lends credence to our claim of the dominance of PO phonon scattering in β -Ga₂O₃.

In a recent work, Parisini and Fornari suggested that intrinsic electron mobility in β -Ga₂O₃ is controlled by optical deformation potential (ODP) scattering.²⁶ It is known that ODP scattering plays an important role in non-polar crystals such as silicon and germanium, and disappears due to symmetry when the CBM is at the Γ point and there are only two atoms in the primitive unit cell.²⁷⁻²⁹ β -Ga₂O₃, with CBM at the Γ point, however

TABLE I. Material parameters of β -Ga₂O₃.

Parameter	Symbol	Value
Mass Density (g/cm ³)	ρ	5.88 ^a
Sound Velocity (cm/s)	v_s	6.8×10^5 ^b
Acoustic Deformation Potential (eV)	D_A	6.9 ^b
Static Dielectric Constant	ϵ_s	10.2 ^c
High-frequency Dielectric Constant	ϵ_∞	3.57 ^c
CBM Electron Effective Mass (m_0)	m_c^*	0.28 ^d
PO Phonon Energy (meV)	$\hbar\omega_0$	44 (fitted)

^a Ref. 26.

^b Ref. 31 and 32.

^c Ref. 33–35.

^d Ref. 2.

has a monoclinic structure with ten atoms in the primitive unit cell, which leads to 30 phonon modes.¹³ Recent DFT calculation indicates that in β -Ga₂O₃, ODP scattering of electrons at low electric field are negligible compared to the PO phonon scattering,³⁰ similar to other polar semiconductors such as GaN and GaAs.^{18,19} Thus, we do not consider ODP further in this work.

To quantify the dominant role of e-PO scattering in β -Ga₂O₃, the lines of Fig 2 were calculated using the relaxation-time approximation (RTA) solution of the Boltzmann transport equation (BTE). Four scattering mechanisms are considered: ionized impurity (II), neutral impurity (NI), PO phonon, and acoustic deformation potential (ADP). The material parameters used in the calculation are listed in Table I.

The RTA solution of BTE gives the average electron drift mobility for carriers moving in 3-dimensions:³⁶

$$\mu_d = \frac{e\langle\tau_m\rangle}{m_p^*} = \frac{e}{m_p^*} \frac{2}{3k_B T} \frac{\int dE \tau_m E^{3/2} f_0(1-f_0)}{\int dE f_0 E^{1/2}}, \quad (2)$$

where E is the electron energy, f_0 is the Fermi-Dirac distribution, and τ_m is the momentum relaxation time. The Hall factor $r_H = \langle\tau_m^2\rangle/\langle\tau_m\rangle^2$ is calculated to obtain the Hall mobility $\mu_H = \mu_d \cdot r_H$ and the Hall electron density $n_H = n/r_H$, where n is the mobile electron density. τ_m due to each individual scattering mechanism is evaluated using Fermi's golden rule. Phonon and neutral impurity scattering are assumed to be unscreened, while ionized impurity scattering is statically screened by free carriers with the reciprocal Debye screening length: $q_D = \sqrt{e^2 n^* / \epsilon_0 \epsilon_s k_B T}$, where n^* is the effective screening carrier density:³⁷ $n^* = n \cdot F_{-1/2}(\eta_C) / F_{1/2}(\eta_C) + (N_D - n - N_A)(n + N_A) / N_D$, where N_D and N_A are the densities of donors and compensated acceptors. $F_j(x)$ is the Fermi integral, $\eta_C = \frac{E_F - E_c}{k_B T}$, E_F is the Fermi level, and E_c the CBM energy. τ_m of ionized impurity scattering is given by Brooks-Herring model:³⁸ $\tau_{II}(k)^{-1} = \frac{e^4 N_I m_p^*}{8\pi \hbar^3 \epsilon_0^2 \epsilon_s^2 k^3} [\ln(1+b) - b/(1+b)]$, where $N_I = n + 2N_A$, $b = 4k^2/q_D^2$. The scattering rate due to neutral impurities is given by:³⁹ $\tau_{NI}^{-1} = 80\pi N_n \hbar^3 \epsilon_0 \epsilon_s / e^2 m_p^*$, where $N_n = N_D - n - N_A$. For ADP scattering: $\tau_{ADP}(k)^{-1} = D_A^2 k_B T m_p^* k / \pi \hbar^3 \rho v_s^2$,

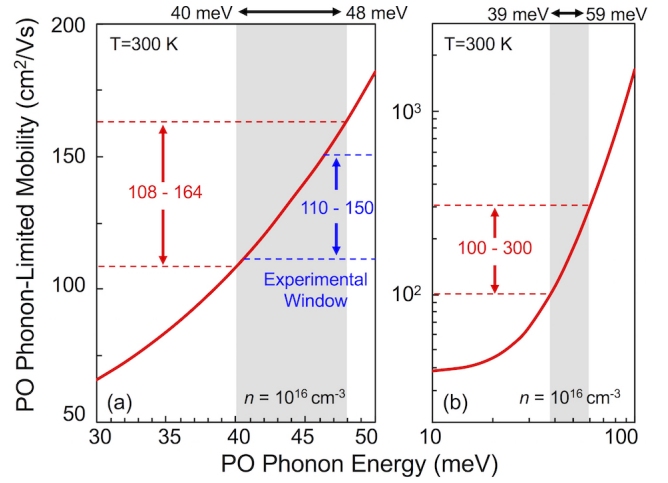


FIG. 3. PO phonon limited electron mobility of β -Ga₂O₃ as a function of $\hbar\omega_0$ at room temperature. Note that (a) is in linear scale and (b) is semi-log scale.

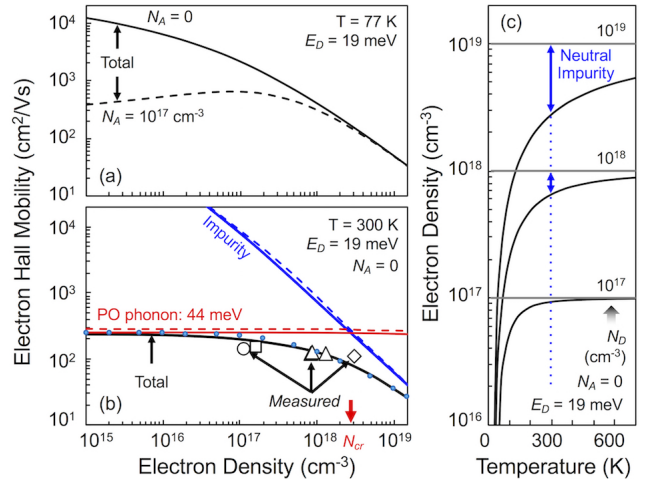


FIG. 4. Electron mobilities as a function of donor concentration at (a) 77 K and (b) 300 K. The symbols show experimental results from different groups: \circ Ref. 15, \triangle Ref. 16, \square Ref. 3, and \diamond Ref. 6. (c) Electron density as a function of temperature with different donor concentrations.

parameters here are defined in Table I. τ_m due to PO phonon scattering is

$$\tau_{PO\pm}(k)^{-1} = \frac{e^2 m_p^* \omega_0}{16\pi \hbar^2 k^3 \epsilon_0} (\epsilon_\infty^{-1} - \epsilon_s^{-1}) (N_0 + 1/2 \pm 1/2) \times \{4kq_0 - 2k_0^2 [\ln(k - q_0) + \ln(k + q_0)]\}, \quad (3)$$

where $q_0 = \sqrt{k^2 \mp k_0^2}$, and $N_0 = [\exp(\hbar\omega_0/k_B T) - 1]^{-1}$ is the equilibrium phonon number. The “+” and “-” subscripts are for PO phonon emission and absorption. The net momentum relaxation rate is obtained using Matthiessen's rule: $\tau_m^{-1} = \tau_{II}^{-1} + \tau_{NI}^{-1} + \tau_{ADP}^{-1} + \tau_{PO}^{-1}$.

Figure 3 shows the the sensitivity of μ_{PO} (drift) to the value of $\hbar\omega_0$ used in Eq. 3 at 300 K. When $\hbar\omega_0$ varies from 40 meV to 48 meV (44 ± 4 meV), μ_{PO} varies

from $108 \sim 164 \text{ cm}^2/\text{V}\cdot\text{s}$. These values fully cover the reported experimental electron mobility values from various groups and are within acceptable experimental errors. Even if we relax the μ_{PO} range to $100 \sim 300 \text{ cm}^2/\text{V}\cdot\text{s}$ (Fig. 3 (b)), where the $300 \text{ cm}^2/\text{V}\cdot\text{s}$ value is the qualitatively estimated intrinsic mobility predicted by Sasaki et al.,⁴⁰ the corresponding $\hbar\omega_0$ ranges from ~ 39 to 59 meV . Therefore $\hbar\omega_0$ in $\beta\text{-Ga}_2\text{O}_3$ that limits electron transport at room temperature is inferred to be not far from $\sim 44 \text{ meV}$ as we have extracted from our experimental results. With the e-PO interaction established as the dominant intrinsic scattering mechanism, it is important to study the relative importance of impurity scattering on electron mobility. Figure 4 (a) and (b) show the calculated μ_H as a function of $N_D - N_A$ at 77 K and 300 K . For 77 K , the solid and dashed lines show mobilities with $N_A = 0$ and $N_A = 10^{17} \text{ cm}^{-3}$. As seen in Fig. 4 (a), intrinsic electron mobility higher than $\sim 10,000 \text{ cm}^2/\text{V}\cdot\text{s}$ can be achieved in very clean samples with $N_D \lesssim 10^{15} \text{ cm}^{-3}$. However, introducing N_A severely

decreases electron mobilities through ionized impurity scattering. When $N_A = 10^{17} \text{ cm}^{-3}$ and $N_D - N_A = 10^{15} \text{ cm}^{-3}$, the mobility is reduced to $\sim 350 \text{ cm}^2/\text{V}\cdot\text{s}$. This explains the experimentally observed low-temperature low electron mobilities,^{3,16} and also much higher mobilities⁴¹ ($\sim 7,000 \text{ cm}^2/\text{V}\cdot\text{s}$) in cleaner samples. In Fig. 4 (b), the black line shows the net μ_H with all four scattering mechanisms considered, the red solid line indicates μ_{PO} with $\hbar\omega_0 = 44 \text{ meV}$ and the blue solid line show mobility limited by ionized and neutral impurity scattering. The open symbols are experimental results from various groups. Figure 4 (c) shows n as a function of temperature for various N_D . The arrows denote the density of neutral impurities. The heavier the doping, the more unionized impurities are introduced. Therefore both ionized and neutral impurity scattering become increasingly important in determining electron mobilities as temperature decreases and as the doping concentration increases.

To estimate μ_H around or higher than 300 K , we derived the following expressions:

$$\mu_{PO} = \frac{e\sqrt{m_p^*}}{\pi^2\hbar^3\omega_0 n \alpha_F k_B T} \times \left[\frac{5}{3N_0} \int_0^{\hbar\omega_0} dE E^{3/2} f_0(1-f_0) + \frac{7}{6(N_0+1)} \int_{\hbar\omega_0}^{\infty} dE E^{3/2} f_0(1-f_0) \right] r_{po}, \quad (4)$$

$$\mu_{II} = \frac{128\sqrt{2\pi}\varepsilon_s^2\varepsilon_0^2(k_B T)^{3/2}}{e^3\sqrt{m_p^*}N_I[\ln(1+\beta^2) - \beta^2/(1+\beta^2)]} r_{ii}, \quad (5)$$

$$\mu_{NI} = e^3 m_p^*/80\pi\hbar^3\varepsilon_s\varepsilon_0 N_n, \quad (6)$$

where $\beta = 2\sqrt{6m_p^*k_B T}/q_D\hbar$, r_{po} and r_{ii} are the Hall factors of PO phonon scattering and ionized impurity scattering, respectively. At 300 K , the empirical expressions $r_{po} = 1.876\{1 + [n(\text{cm}^{-3})/2 \times 10^{19}]^{1.22}\}$ and $r_{ii} = 0.99/1 + [n(\text{cm}^{-3})/3.2 \times 10^{18}]^{0.68} + 0.8$ are used to describe the doping dependence of Hall factors. The first and second terms in the brackets of Eq. 4 correspond to the PO phonon absorption and emission, respectively.

The dashed lines in Fig. 4 (b) show the net μ_H calculated using Eq. 4-6. At 300 K , PO phonon scattering dominates the mobility for N_D lower than a critical doping density N_{cr} determined by the crossover condition $\mu_{PO} \approx (\mu_{II}^{-1} + \mu_{NI}^{-1})^{-1}$. When $N_D > N_{cr}$, neutral impurity introduced by heavy doping severely degrades the electron mobility. For 300 K , $\mu_{PO} \sim 250 \text{ cm}^2/\text{V}\cdot\text{s}$ and $N_{cr} \sim 2.76 \times 10^{18} \text{ cm}^{-3}$. For power devices that typically operate at high temperatures, μ_H is captured by the empirical expression:

$$\mu_H = \frac{56 \left\{ \exp\left[\frac{508}{T(\text{K})}\right] - 1 \right\}}{\left\{ 1 + \frac{N_D(\text{cm}^{-3})}{[T(\text{K}) - 278]2.8 \times 10^{16}} \right\}^{0.68}} \frac{\text{cm}^2}{\text{V}\cdot\text{s}}. \quad (7)$$

The 300 K electron mobility calculated using Eq. 7 is shown by blue dots in Fig. 4 (b). This expression, which

is valid for $300 \text{ K} \lesssim T \lesssim 500 \text{ K}$, offers a useful guideline for experiments and is easily embedded in device modeling.

In summary, we studied the intrinsic electron mobility limits in n -doped $\beta\text{-Ga}_2\text{O}_3$. We find an extremely strong Fröhlich interaction in the material, fueled by the high ionicity of the chemical bonds, and the low optical phonon energies. A PO phonon energy of $\sim 44 \text{ meV}$ was deduced from the transport properties. The measured room-temperature electron mobility is dominated by PO phonon scattering for low doping densities, and thus has approached the intrinsic mobility limits. Though it is difficult to change the PO phonon energy, one could investigate strain as a potential tool.⁴² Moreover, similar to III-V semiconductors, the formation of a two-dimensional electron gas (2DEG) at $(\text{AlGa})_2\text{O}_3/\text{Ga}_2\text{O}_3$ heterojunctions is possible with modulation doping. The electron mobility in such a 2DEG is expected to be higher than the bulk due to the relaxation of the momentum conservation in the direction perpendicular to the interface during the electron-PO phonon scattering process, the elimination of neutral impurity potential, and the powerful exponential reduction of ionized impurity scattering by remote doping.

ACKNOWLEDGMENTS

This work was supported by NSF DMREF program (Award Number 1534303). The authors thank Guru Khalsa for useful discussions.

- ¹H. H. Tippins, Phys. Rev. 140, A316 (1965).
- ²J. B. Varley, J. R. Weber, A. Janotti, and C. G. Van de Walle, Appl. Phys. Lett. 97, 142106 (2010).
- ³T. Oishi, Y. Koga, K. Harada, and M. Kasu, Appl. Phys. Express 8, 031101 (2015).
- ⁴M. Higashiwaki, K. Sasaki, H. Murakami, Y. Kumagai, A. Koukitsu, A. Kuramata, T. Masui, and S. Yamakoshi, Semicond. Sci. Technol. 31, 034001 (2016).
- ⁵K. Sasaki, M. Higashiwaki, A. Kuramata, T. Masui, and S. Yamakoshi, J. Crystal Growth 378, 591 (2013).
- ⁶W. S. Hwang, A. Verma, H. Peelaers, V. Protasenko, S. Rouvimov, H. G. Xing, A. Seabaugh, W. Haensch, C. Van de Walle, Z. Galazka, et al., Appl. Phys. Lett. 104, 203111(2014).
- ⁷E. Fortunato, P. Barquinha, and R. Martins, Adv. Mater. 24, 2945 (2012).
- ⁸A. Ohtomo and H. Y. Hwang, Nature 427, 423 (2004).
- ⁹R. L. Hoffman, B. J. Norris, and J. F. Wager, Appl. Phys. Lett. 82, 733 (2003).
- ¹⁰C. Hermann and C. Weisbuch, Phys. Rev. B 15, 823 (1977).
- ¹¹J. T. Devreese, V. M. Fomin, E. P. Pokatilov, E. A. Kotomin, R. Eglitis, and Y. F. Zhukovskii, Phys. Rev. B. 63, 184304 (2001).
- ¹²S. Adachi, *Properties of Group-IV, III-V and II-VI Semiconductors* (Wiley, Chichester, 2005).
- ¹³K. Yamaguchi, Solid State Commun. 131, 739 (2004).
- ¹⁴E. G. Vllora, K. Shimamura, T. Ujiie, and K. Aoki, Appl. Phys. Lett. 92, 202118 (2008).
- ¹⁵Z. Galazka, R. Uecker, K. Irmscher, M. Albrecht, D. Klimm, M. Pietsch, M. Brützm, R. Bertram, S. Ganschow, and R. Fornari, Cryst. Res. Technol. 45, 1229 (2010).
- ¹⁶K. Irmscher, Z. Galazka, M. Pietsch, R. Uecker, and R. Fornari, J. Appl. Phys. 110, 063720 (2011).
- ¹⁷H. He, M. A. Blanco, and R. Pandey, Appl. Phys. Lett. 88, 261904 (2006).
- ¹⁸B. K. Ridley, B. E. Foutz, and L. F. Eastman, Phys. Rev. B 61, 16862 (2000).
- ¹⁹K. Hirakawa and H. Sakaki, Phys. Rev. B 33, 8291 (1986).
- ²⁰K. Seeger, *Semiconductor Physics* (9th Edition, Springer, New York, 2004).
- ²¹H. Fröhlich, *Advances in Physics* 3, 325 (1954).
- ²²L. Pauling, *The Nature of the Chemical Bond* (3rd Edition, Cornell University Press)
- ²³T. Onuma, S. Saito, K. Sasaki, K. Goto, T. Masui, T. Yamaguchi, T. Honda, A. Kuramata, and M. Higashiwaki, Appl. Phys. Lett. 108, 101904 (2016).
- ²⁴A. Norman Jette, T. L. Gilbert, and T. P. Das, Phys. Rev. 184, 884 (1969).
- ²⁵B. L. Gelmont, M. Shur, and M. Stroschio, J. Appl. Phys. 77, 657 (1995).
- ²⁶A. Parisini and R. Fornari, Semicond. Sci. Technol. 31, 035023 (2016).
- ²⁷B. K. Ridley, *Quantum Processed in Semiconductors* (4th Edition, Clarendon Press, Oxford, 1999).
- ²⁸R. Seitz, Phys. Rev. 73, 549 (1948).
- ²⁹W. A. Harrison, Phys. Rev. 104, 1281 (1956).
- ³⁰K. Ghosh and U. Singiseti, Appl. Phys. Lett. 109, 072102 (2016).
- ³¹Z. Guo, A. Verma, X. F. Wu, F. Y. Sun, A. Hickman, T. Masui, A. Kuramata, M. Higashiwaki, D. Jena, and T. F. Luo, Appl. Phys. Lett. 106, 111909 (2015).
- ³²The deformation potential D_{α}^i of a particular band i induced by a certain phonon mode α through electron-phonon interaction is given by $D_{\alpha}^i = \Delta V_i / (\Delta l_{\alpha} / l_0)$, where ΔV_i is the energy change of band i relative to that in the equilibrium structure, l_0 is the lattice constant of the equilibrium structure, and Δl_{α} is the lattice constant change due to a structural perturbation from phonon mode α . The calculation is carried out by first displacing the atomic coordinates in the optimized cell from their equilibrium positions by a small amount through following the eigenvector of a certain phonon mode. The band-structure calculation is then performed on a series of such deformed structures with different Δl_{α} ($-0.01l_0$ to $0.01l_0$). The deformation potential for the band gap $\Delta V_{bg} = \Delta V_{CBM} - \Delta V_{VBM}$ is thus obtained by a linear fit of ΔV_{bg} versus $\Delta l_{\alpha} / l_0$. The first-principles calculation details were described in 31
- ³³M. Passlack, N. E. J. Hunt, E. F. Schubert, G. J. Zyzdik, M. Hong, J. P. Mannaerts, R. L. Opila, and R. J. Fischer, Appl. Phys. Lett. 64, 2715 (1994).
- ³⁴M. Passlack, E. F. Schubert, W. S. Hobson, M. Hong, N. Moriya, S. N. G. Chu, K. Konstadinidis, J. P. Mannaerts, M. L. Schnoes, and G. J. Zyzdik, J. Appl. Phys. 77, 686 (1995).
- ³⁵M. Rebien, W. Henrion, M. Hong, J. P. Mannaerts, and M. Fleischer, Appl. Phys. Lett. 81, 250 (2002).
- ³⁶C. Hamaguchi, *Basic Semiconductor Physics* (2nd Edition, Springer, 2010).
- ³⁷C. M. Wolfe, N. Holonyak Jr., G. E. Stillman, *Physical Properties of Semiconductors* (1st Edition, Prentice Hall, 1989).
- ³⁸D. Chattopadhyay and H. J. Queisser, Rev. Mod. Phys. 53, 745 (1981).
- ³⁹C. Erginsoy, Phys. Rev. 79, 1013 (1950).
- ⁴⁰K. Sasaki, A. Kuramata, T. Masui, E. G. Vllora, Appl. Phys. Exp. 5, 035502 (2012).
- ⁴¹Private communication with Y. Kumagai, Tokyo University of Agriculture and Technology, Koganei, Tokyo 184-8588, Japan.
- ⁴²M. Qi, G. W. Li, V. Protasenko, P. Zhao, J. Verma, B. Song, S. Ganguly, M. D. Zhu, Z. Y. Hu, X. D. Yan, et al., Appl. Phys. Lett. 106, 041906 (2015).